Structure and Bonding of the Multifunctional Amino Acid L-DOPA on Au(110)

M. Weinhold,[†,‡] S. Soubatch,[†] R. Temirov,[†] M. Rohlfing,[§] B. Jastorff,[‡] F. S. Tautz,*,[†] and C. Doose[†,‡]

School of Engineering and Science, International University Bremen, Campus Ring 8, 28759 Bremen, Germany, Zentrum für Umweltforschung und Umwelttechnologie, Universität Bremen, Leobener Strasse, 28359 Bremen, Germany, and Fachbereich Physik, Universität Osnabrück, Barbarastrasse 7, 49069 Osnabrück, Germany

In investigations of the proteins which are responsible for the surface adhesion of the blue mussel *Mytilus edulis*, an unusually frequent appearance of the otherwise rare amino acid 3-(3,4-dihydroxyphenyl)-L-alanine (L-DOPA) has been observed. This amino acid is thought to play a major role in the mechanism of mussel adhesion. Here we report a detailed structural and spectroscopic investigation of the interface between L-DOPA and a single-crystalline Au(110) model surface, with the aim of understanding fundamentals about the surface bonding of this amino acid and its role in mussel adhesion. Molecular layers are deposited by organic molecular beam deposition (OMBD) in an ultrahigh-vacuum environment. The following experimental techniques have been applied: ex situ Fourier transform infrared spectroscopy (FTIR), X-ray photoelectron spectroscopy (XPS), low-energy electron diffraction (LEED), high-resolution electron energy loss spectroscopy (HREELS), and scanning tunneling microscopy (STM). Vibrational spectra of isolated L-DOPA molecules and the zwitterionic bulk have been calculated using density functional theory (DFT). The predicted modes are assigned to observed spectra, allowing conclusions regarding the molecule−substrate and molecule−molecule interactions at the L-DOPA/Au(110) interface. We find that zwitterionic L-DOPA forms a monochiral, one-domain commensurate monolayer on Au(110), with the catechol rings on top of [$1\bar{1}0$] gold rows, oriented parallel to the surface. The (2×1)-Au(110) surface reconstruction is not lifted. The carboxylate group is found in a bidentate or bridging configuration, the amino group is tilted out of the surface plane, and the hydroxyl groups do not dehydrogenate on Au(110). Similar to the case for the bulk, molecules form dimers on Au(110). However, the number of hydrogen bridge bonds between L-DOPA molecules is reduced as compared to the bulk. Thicker layers which deposited onto the commensurate interface do not order in the bulk structure. In conclusion, our study shows that the aromatic ring system of L-DOPA functions as a surface anchor. Since it is also known that the hydroxyl groups support cross-link reactions between L-DOPA residues in the mussel glue protein, we can conclude that the catechol ring supports surface adhesion of mussel proteins via two independent functions.

1. Introduction

In recent years, the adhesive strategies of the blue mussel *Mytilus edulis* have aroused interest, due to its matchless ability to attach to almost any available surface, even in wet and salty environments.[1−8] A number of investigations directed at the blue mussel's adhesive foot proteins have revealed an unusually frequent appearance of the otherwise rare amino acid 3-(3,4-dihydroxyphenyl)-L-alanine (L-DOPA).[8−11] Hence, this amino acid is thought to play a major role in the mechanism of mussel adhesion: first, due to its ability to support cross-link reactions in the protein,[12−14] and second, due to its ability to form interfacial chemisorption complexes.[15−17] Various reactions of L-DOPA side chains embedded in a peptide or protein, namely oxidation, imine formation, Michael adduct formation, radical generation, radical coupling, and metal chelation, are possible, and indeed some of them are deemed responsible for the good adhesive properties of mussel foot proteins. Most notably, ferric

ions have shown a strong curing effect on mussel peptides, due to their ability to form complexes with the aromatic residues of various L-DOPA components in the peptides.[18,19]

Fueled by research into antifouling strategies and biomimetic adhesion, a growing interest in the application of protein/surface adhesion mechanisms has arisen. Unfortunately, these mechanisms are as yet poorly understood. A clear distinction of the contribution of the L-DOPA molecule itself (and especially its catechol ring) on one hand and the peptide structure on the other would be a key step toward a better understanding of protein/surface adhesion of the blue mussel's foot proteins. Hence, the adsorption properties of the isolated L-DOPA molecule have to be considered. Adsorption experiments on the single amino acid are complementary to experiments involving peptides and proteins, and at the same time they are a good basis for detailed investigations of these more complex adsorbates. In the present work we have therefore chosen the single L-DOPA molecule as our starting point for a systematic investigation of molecular interaction potentials (MIP) upon adsorption of mussel proteins on metal surfaces. Recently, Jastorff et al.[20,21] showed that valuable information on physicochemical properties of a sub-

* To whom correspondence should be addressed. E-mail: s.tautz@iu-bremen.de.
† International University Bremen.
‡ Universität Bremen.
§ Universität Osnabrück.

stance can be deduced from its molecular structure by specifying and considering its molecular interaction potentials.

The goal of the present work is to experimentally identify the behavior of this amino acid when it is adsorbed on an *inert* metal surface. The use of an inert substrate can help us to distinguish L-DOPA's various molecular interaction potentials without the effect of the surface on the unprotected amino acid being too strong. More reactive metal surfaces may modify the amino acid at one or more of its functional groups. The (110) surface of gold was chosen because the atomic structure of the (2×1) reconstructed surface,[22,23] consisting of alternating rows of grooves and ridges along the [1$\bar{1}$0] direction, can be expected to induce a templating effect, stimulating an ordered structure of the adsorbed L-DOPA layer. Since in highly ordered layers molecules are situated in a well-defined environment, surface analytical investigations can reveal even subtle details of the interaction between the molecular adsorbate and the metallic substrate, which clearly is beneficial for the overall aim of the present work.

We have carried out our study of the surface behavior of L-DOPA under ultrahigh-vacuum (UHV) conditions, because in this way highly informative surface analysis techniques such as X-ray photoelectron spectroscopy (XPS), low-energy electron diffraction (LEED), scanning tunneling microscopy (STM), and high-resolution electron energy-loss spectroscopy (HREELS) can be applied to the problem. Of course, the real situation of an adhesive protein involves the presence of water, which may modify the chemical molecule−surface interaction. Thus, care must be taken if an extension of the findings reported here to biologically relevant ambients is sought.

L-DOPA (cf. Figure 1 for the chemical structure) contains several elements (N, O, C, H) and functional groups (hydroxyl, amino, and carboxylate or acid groups) and provides several molecular interaction potentials:[20,21] H-donor, H-acceptor, charge transfer, and hydrophobic potentials, as well as dipole moments and positive and negative charges. The molecule also exhibits the chiral center which is found in all amino acids apart from glycine (marked with an arrow in Figure 1a). A further important aspect of all amino acids is that their charging state may vary from uncharged to anionic, cationic, or zwitterionic, according to the environment they are exposed to.[24] Most commonly, they are zwitterionic in the bulk crystalline structure[25−27] and uncharged in their isolated gaseous state,[28,29] whereas in solution, their state depends on the pH value, varying from cationic through zwitterionic to anionic as the acidity decreases.[30] Thus, an important point to address is the charging state adopted by the molecule upon adsorption on Au(110).

We note here that, in an adhesive protein, the amino acid is present in its protected form (no free amino or acid groups). This will of course modify the interaction of the molecule with the substrate. However, experiments on the unprotected amino acid are useful as a reference to understand how the loss of free amino and acid groups changes the molecule−substrate interaction. Further experiments for the protected amino acid are planned.

Several simple amino acids (e.g. glycine,[31−41] alanine,[41−50] proline,[41,51,52] cysteine,[41,53,54] and methionine[41]) have been studied thoroughly with a spectrum of vacuum-based surface sensitive techniques which give access to information on the atomic scale.[55] In contrast, only a few studies have been reported for the interactions between L-DOPA and metals so far. This lack of detailed experiments is at least in part a consequence of the difficulty in preparing highly pure thin films of L-DOPA in situ by physical vapor deposition (cf. section 2). Oliveri et al.[15]
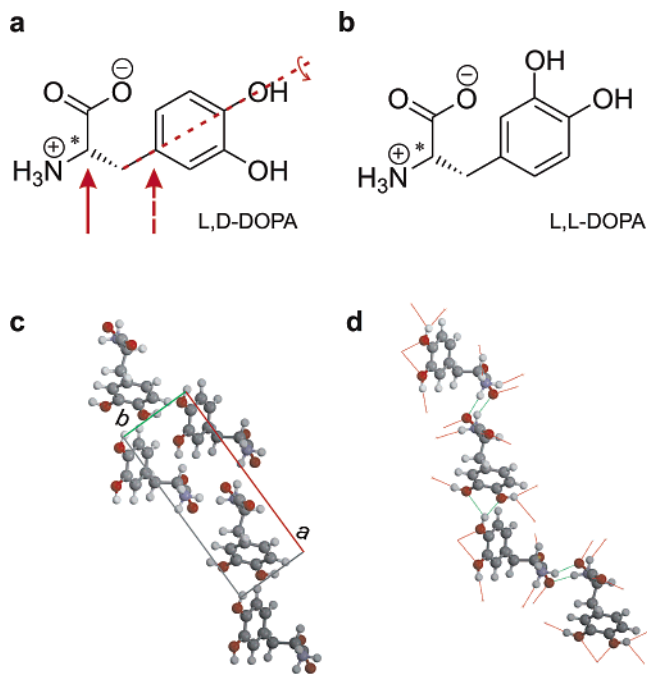

Figure 1. (a) Structure formula of 3-(3,4-dihydroxyphenyl)-L-alanine (L-DOPA). The solid red arrow indicates the intrinsic chiral center of the molecule. The red dashed arrow indicates the center, which becomes chiral if the catechol ring adsorbs flat on a surface: if the latter is rotated by 180° around the red dashed axis, a second surface species (L,L-DOPA) results, as shown in (b). The first letter specifies the intrinsic chirality and the second the surface-induced chirality. (c) Bulk crystal structure of L-DOPA (low-temperature phase). The unit cell with $a = 13.619$ Å, $b = 5.232$ Å, $c = 6.062$ Å, $\alpha = 90°$, $\beta = 97.56°$, and $\gamma = 90°$ is indicated.[26] The c axis is perpendicular to the plane of the paper. (d) In the bulk structure, molecules form chains with a head-to-head and tail-to-tail structure. This structure is stabilized by hydrogen bonds involving the hydroxyl, carboxylate, and amino groups. The hydrogen bridges are shown as thin lines.

investigated the adsorption of L-DOPA-containing peptides and suggested that L-DOPA is their primary binding unit to the surface. On the basis of multiply attenuated internal reflection infrared spectroscopy (MAIR-IR) they concluded that the catechol ring lies flat on the germanium surface. Analyzing data from electron energy loss spectroscopy (EELS) and Auger electron spectroscopy (AES), Stern et al.[16] suggested a parallel orientation of the phenylene ring on Pt(100) and Pt(111) surfaces after deposition from solutions. They further suggested that L-DOPA adsorbs in the uncharged state and binds with the acid and the hydroxyl groups to the underlying metal; hence, the molecule is dehydrogenated upon hydroxyl−surface bond formation. Ooka et al.[17] deposited L-DOPA from solution and investigated L-DOPA-containing mussel peptide sequences using surface-enhanced Raman scattering (SERS). In contrast to the findings cited above, they concluded that L-DOPA binds edge-on to colloidal gold particles, again via dehydrogenation of its hydroxyl groups.

This paper is organized as follows: in the next section experimental details of the present work will be reported, with special emphasis on the deposition protocol of L-DOPA by organic molecular beam deposition (OMBD), because successful application of OMBD to L-DOPA is crucial for achieving the goals of the present study. In the third section, experimental and theoretical results will be discussed, starting with a proof in sections 3.1 (vibrational fingerprint) and 3.2 (chemical composition) that the deposit of the OMBD experiment is indeed L-DOPA and followed by the discussion of the molecular structure of the L-DOPA/Au(110) interface on the basis of

23758 *J. Phys. Chem. B, Vol. 110, No. 47, 2006*

Weinhold et al.

electron diffraction experiments in section 3.3. In section 3.4, the vibrational properties of L-DOPA in its various states (separate molecule, bulk material, and adsorbed monolayers and multilayers), are reported, on the basis of both infrared spectroscopy (FTIR) and inelastic electron scattering (HREELS) experiments and density functional (DFT) calculations. In this section, vibrational modes are assigned, and from some of the characteristic features of the vibrational spectra of L-DOPA/Au(110) monolayers conclusions regarding the chemical state, the molecular orientation and conformation, and the molecule−substrate and molecule−molecule interactions in the adsorbed layer are drawn. In section 3.5, the results of molecularly resolved real-space imaging of the L-DOPA/Au(110) interface are reported, and—gathering all available experimental and theoretical information—a comprehensive structural model for this interface is developed in section 3.6. Finally, in section 4 the implications of our findings for the problem of bioadhesion are briefly discussed.

2. Experimental Methods

Experiments have been performed in an ultrahigh-vacuum (UHV) system equipped with a HREELS spectrometer (Delta 0.5, Specs GmbH), a 3-grid LEED optics (ErLEED 150, Specs GmbH), a hemispherical analyzer for photoelectron spectroscopy (Phoibos 100, Specs GmbH), an ion-sputtering gun and a 1−300 amu quadrupole mass spectrometer (QMS, Pfeiffer Vakuum GmbH). Scanning tunneling experiments have been conducted in a second UHV vessel furnished with a low-temperature scanning tunneling microscope (VTS-Createc GmbH) and a LEED optics (Schaefer Technologie GmbH).

3-(3,4-Dihydroxyphenyl)-L-alanine (L-DOPA), CAS [59−92−7], was purchased from Fluka (Buchs, Switzerland). L-DOPA was deposited onto the Au(110)(2 × 1) surface using organic molecuar beam deposition (OMBD) from a homemade effusion cell. Prior to use, the commercial material was thoroughly outgassed at 390 K under UHV for 20 h. Afterward the filled effusion cell was heated to 490 K over a period of 30 min and held at 490 K for 1 h. OMBD of L-DOPA requires very precise temperature control, because under vacuum conditions the sublimation point and the decomposition point of the material are very close to each other. Nevertheless, after systematic experiments it has turned out that OMBD of L-DOPA without additional contamination by decomposition products is possible, if the deposition protocol is closely adhered to. Thorough outgassing is mandatory. The heating ramp must be slow (6−7 K/min), such that overheating of the L-DOPA charge in the Knudsen cell is avoided. First evaporation is observed at 490 ± 10 K. At about 520 ± 10 K, L-DOPA decomposes, leaving behind black material in the crucible. Temperatures higher than 510 K lead to a 2−3-fold increase in the powder volume on melting, followed by decomposition. Varying the deposition time, layers of different thicknesses were grown. Growth rates of approximately 1 Å/min have been achieved at 490−500 K. At this temperature, the initially white powder turns into a beige sintered material, from which L-DOPA layers can be evaporated. Infrared spectroscopy has been employed to verify that the deposit is intact L-DOPA.

The Au(110)(2 × 1) surface was cleaned in situ by the conventional procedure of repeated sputter−anneal cycles. For sputtering, the Au crystal was bombarded for 15 min with 1 keV Ar$^+$ ions at room temperature (RT), yielding a target current of 50 μA at a partial Ar pressure of approximately 4 × 10^{-5} mbar. After the treatment the surface was annealed 10 min at 700 K followed by slow cooling to RT. Between

these cycles the surface quality was checked with LEED and XPS. The Au(110) crystal onto which L-DOPA was deposited showed a sharp (2 × 1) missing row reconstruction. No carbon or oxygen contaminations were detected with XPS.

Our film-thickness calibration relies on the combination of quadrupole mass spectrometry (QMS) during evaporation and in situ XPS. Molecular fragments with 110 and 123 amu were observed in the QMS during evaporation. These fragments are produced by the ionization process in the QMS. The 110 amu fragment is the protonated residual catechol ring without the carbon chain, while the 123 amu fragment is the catechol ring with the residual CH$_2$ group from the chain. The onset of evaporation is indicated by the appearance of these mass signals. A gate valve was used as a shutter to control the deposition times.

Measurements of layer thicknesses were performed with XPS. For each of the films, the photoelectrons of the Au 4f and C 1s core levels, excited by Al Kα X-rays, have been recorded. Peak areas were determined by CASAXPS[56] and used as input data for MULTIQUANT,[57] a program which calculates the layer thickness in a homogeneous surface layer model from the strength of the overlayer and substrate signals. Relative sensitivity factors based on Wagner et al.[58] have been employed in the fitting. Furthermore, the O 1s and C 1s signals have been recorded with high resolution, enabling the analysis of characteristic core-level shifts due to differently bonded atoms in the molecule. High-resolution photoelectron spectra were fitted with CASAXPS. Gauss−Lorentz profiles with 0.3/0.7 Gaussian/Lorentzian contribution and a Shirley background[59] have been used.

Vibrational spectroscopy of thin films was carried out both ex situ with an FT-IR spectrometer of the type Nicolet Aratar 370 (Thermo Electron Corp., Waltham, MA) and in situ with a HREELS spectrometer. For IR experiments, L-DOPA was deposited under UHV onto a KBr pellet which was transferred through air and loaded into the IR spectrometer afterward. For HREELS, a monochromatic electron beam with 4 eV primary energy was used. Routinely, an energy resolution of 3−4 meV full-width at half-maximum was achieved for the elastic peak. HREELS spectra presented here have been collected in specular geometry, which corresponds to the dipole scattering mechanism.

The angular distribution of dipole scattered electrons in HREELS is sharply peaked around the specular direction. The so-called surface selection rule states that only modes belonging to totally symmetric representations can be observed in dipole scattering.[60] Because of the low symmetry of the L-DOPA molecule (group I), all vibrational modes in fact belong to the totally symmetric representation. Strictly speaking, the surface selection rule, therefore, cannot be applied in the case of L-DOPA adsorption. However, it is still true that modes for which the dynamic dipole moment is parallel or nearly parallel to the surface will be strongly suppressed, because of the near-cancellation of the dynamical dipole in the molecule by its image in the metal surface. For in-plane modes the surface selection rule hence survives in weakened form as a propensity rule. In this form, it can indeed be used to deduce the orientation of certain parts of the L-DOPA molecule on Au(110).

The STM experiments were carried out in a second UHV machine. Nevertheless, the preparation of L-DOPA layers was carried out using the same effusion cell and according to the same protocol as for the spectroscopic experiments. After deposition, the sample was cooled to 100 K and transferred into the cold STM (T = 6 K).

To aid our interpretation of the complex vibrational spectra, the vibrational frequencies were theoretically calculated for an isolated molecule and for the bulk structure. The bulk structure was taken from ref 26. For the isolated uncharged molecule, the basis set cc-pVQZ[61] of GAUSSIAN[62] (B3PW91 functional) was used. In a first step, DFT calculations of the electronic structure of the molecule were carried out to generate the equilibrium structure of the molecule.

In addition to DFT studies with GAUSSIAN, the structure, vibrations, and related infrared intensities of both the free molecule and the zwitterionic bulk structure were also investigated using the SIESTA package.[63,64] The relaxed structure of the free molecule, calculated with SIESTA, was found to be in good agreement with the results of GAUSSIAN. For the relaxation of the bulk structure, we have started from the experimentally known unit cell (see Figure 1) and atoms therein. Atomic positions were relaxed until all forces on the atoms are zero. This is necessary to be able to calculate force constants for vibrations. The observed atomic relaxations from the experimental data are small (0.12 Å at most). We have also started the bulk calculation from the structure of the free molecule. Here, relaxation to the zwitterionic state occurred without barrier, accompanied by an energy gain, clearly demonstrating the instability of the free-molecule geometry in the condensed state. After geometric relaxation, all force constants were calculated, and the dynamic matrix at zero momentum was set up. The force constants were calculated by averaging the forces arising when an atom is displaced by 0.021 Å in the forward and backward directions. Again, this was done for the free molecule as well as for the bulk structure, finally allowing us to calculate the vibrational frequencies and corresponding displacement patterns. In the case of the free molecule, the results from SIESTA are in good agreement with the data from GAUSSIAN.

On the basis of the displacement pattern of each vibrational mode, its infrared activity was simulated. To this end, we have evaluated the change in the polarization when the structure is displaced from its equilibrium along each of the eigenmode elongation patterns. In this procedure, the mode amplitudes were chosen such that the increase of elastic energy equals $\hbar\omega$ (i.e. one vibrational quantum) of the mode. Again, this was done for the free molecule and for the bulk structure, using the SIESTA package. In the case of the infrared spectrum of the free molecule, good agreement with the infrared activity data from GAUSSIAN was found.

Calculated spectra have been broadened with Gauss/Lorentz profiles to ease comparison with experimental spectra. Because the calculated frequencies may deviate systematically from the experimental ones by a common factor, we have rescaled the theoretical frequency axis to achieve optimum agreement with experimental data. Here the agreement was quantified by a Pendry R_P factor analysis.[65,66] To this purpose, experimental HREELS and FT-IR spectra have been compared with frequency-scaled and broadened (10 cm^{-1} for comparison with HREELS and 5 cm^{-1} for comparison with IR) calculated spectra for the bulk zwitterionic state. When the scaling factor was varied, a local minimum of reliability R_P factor was found at a scaling of 0.992. Correspondingly, all the computed frequencies for the zwitterionic state quoted in this paper have been scaled by this factor.

3 Results and Discussion

3.1. Organic Molecular Beam Deposition. The first issue to be addressed is the feasibility of depositing L-DOPA by
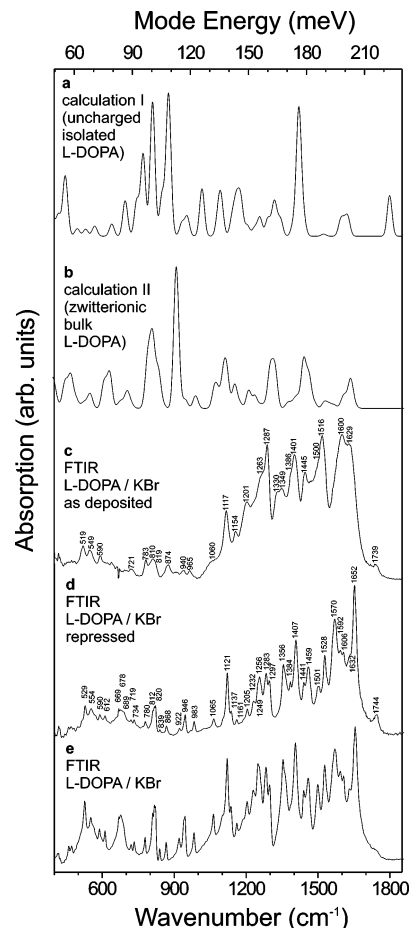
Figure 2. Comparison of DFT-calculated vibrational spectra for (a) the uncharged isolated L-DOPA molecule and (b) the zwitterionic L-DOPA bulk crystal with (c) IR spectra of L-DOPA as deposited on a KBr pellet and (d) IR spectra of the deposited material after crushing and repressing into a KBr pellet. The last spectrum is essentially identical with the reference spectrum of clean L-DOPA powder (e). The theoretical spectra in parts a and b have been broadened by Gaussians with $\sigma = 10$ cm^{-1}. For more information see the text.

organic molecular beam deposition. This feasibility is far from obvious, because initial experiments have shown that the sublimation temperature ($T = 490 \pm 10$ K) and the decomposition temperature of L-DOPA ($T = 520 \pm 10$ K) are very close. A likely reason for the high sublimation temperature is the relatively strong cohesion of the solid material, caused by hydrogen bonds in the zwitterionic bulk structure (Figure 1c,d). It has already been mentioned in the Experimental Section that, despite these difficulties, a successful OMBD deposition protocol has been developed after extensive trial experiments. In the present section, we describe the experiments which prove that the films deposited according to this protocol indeed consist of intact L-DOPA molecules. Ex situ FT-IR experiments and in situ XPS experiments have been used to this purpose.

Figure 2c displays an infrared spectrum of the fingerprint region of a thin film, deposited from the L-DOPA source onto a KBr pellet according to the protocol described above. If this spectrum is compared to a reference spectrum of L-DOPA powder, mixed with KBr and pressed into a pellet (Figure 2e), characteristic differences between the two spectra are evident. The question thus arises whether L-DOPA or a modified compound have been deposited. A detailed analysis shows that the spectrum in Figure 2c indeed corresponds to a pure L-DOPA film.

(1) Figure 2d shows the spectrum of the same molecular material as in Figure 2c, but after repressing the pellet. The material of the thin film is now homogeneously dispersed in a matrix of KBr microcrystallites. Apparently, the dispersion modifies the vibrational fingerprint of the deposited material, which is now nearly identical with the fingerprint of the original L-DOPA before sublimation (Figure 2e). Hence, we can conclude that the OMBD-deposited film consists of intact L-DOPA molecules.

(2) Figure 2 also displays two simulated vibrational spectra. Figure 2a gives the calculated spectrum of an uncharged, isolated molecule, calculated with GAUSSIAN. Figure 2b, on the other hand, shows the calculated spectrum of crystalline L-DOPA, calculated by SIESTA code as described in section 2. For ease of comparison with the experimental spectra in Figure 2, both theoretical spectra have been broadened with Gauss/Lorentz profiles of $10 \ cm^{-1}$ width. We note marked differences between the two simulated spectra across the whole fingerprint region. At the same time, a better agreement between the experimental spectrum of the as-deposited film (Figure 2c) and the calculation of the zwitterionic crystalline material (Figure 2b) is found than for the calculation of the free molecule (Figure 2a). This indicates that crystalline, zwitterionic L-DOPA has most likely been deposited, in agrement with the results of similar studies of other amino acids,[25−27] although the degree of concurrence between the spectra in parts b and c of Figure 2 is not perfect. Additionally we note that embedding the molecule in a microcrystalline KBr matrix leads to a substantial change of the vibrational fingerprint.

In conclusion, the analysis of the vibrational fingerprint region proves that the deposition protocol discussed in section 2 allows us to deposit L-DOPA films on arbitrary substrates by vacuum sublimation. The analysis of XPS core-level spectra, presented in the next section, confirms this conclusion.

3.2 Chemical Composition of the Deposited Film. The chemical composition of the film was analyzed with X-ray photoelectron spectroscopy. Both C 1s and O 1s core level spectra have been recorded. This was followed by a detailed line shape analysis, with the aim of excluding any significant contamination of the as-deposited L-DOPA film on Au(110). Note that prior to L-DOPA deposition it has been confirmed by XPS that no carbon or oxygen contamination is present on the freshly prepared Au(110) surface. The results of the peak fitting are displayed in Figure 3.

At first sight, the C 1s peak in Figure 3a exhibits three clearly distinct features within the binding energy range 283−290 eV and a further broad feature around 292 eV. In a three-peak fit, these correspond to aromatic carbon at 284.5 eV (C1), carbon attached to a hydroxyl group at 286.1 eV (C3), and carboxylate carbon at 288.5 eV (C5). A detailed analysis, however, reveals that with additional components the quality of the peak fit can be improved substantially. Theoretically, five peaks are to be expected, because L-DOPA contains five distinct carbon species: i.e., one additional peak each for the aliphatic carbon C2 and the carbon attached to the amino group C4. We have therefore fitted the C 1s spectrum with five peaks. We note the very good agreement between the peak positions of the fitted components in Figure 3a with equivalent carbon species reported for other amino acids or related compounds in the literature (cf. Table 1 and below). Since the energy regions to which our component peaks have been confined are 2.0 eV, this agreement—together with the very good accordance of the relative peak intensities with the stoichiometry of the molecule—confirms the presence
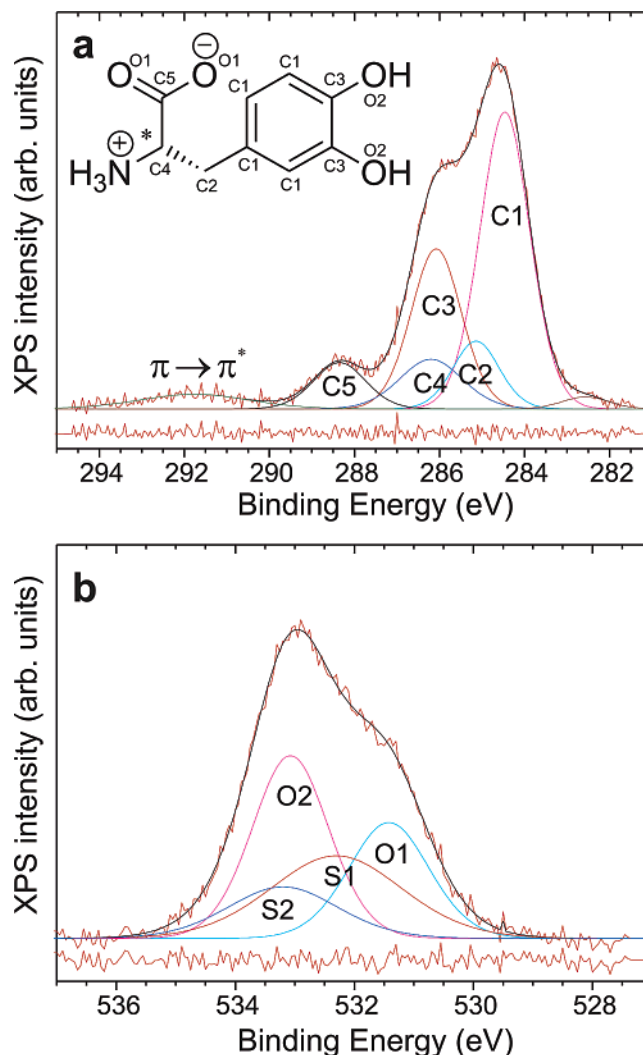

Figure 3. XPS spectra for the (a) C 1s and (b) O 1s regions of an L-DOPA film of approximately 500 Å thickness. Spectra were recorded with Al Kα excitation and 5 eV pass energy. Labels C1−C5 and O1 and O2 refer to carbon and oxygen species in different chemical environments, as shown in the inset. For the O 1s spectra, one satellite each for the two species O1 and O2 was necessary to obtain a satisfactory fit of the experimental peak profile.

TABLE 1: Results of the C 1s and O 1s Peak Fitting

	percentage		position (eV)	
	theory	expt	lit.	expt
C1	44.4	43.9	284.4[67]	284.5
C2	11.1	9.3	284.7[68]	285.1
C3	22.2	23.9	286.0[69]	286.1
C4	11.1	9.3	286.3[69]	286.2
C5	11.1	7.2	289.0[31]	288.4
O1	50.0	50.6	531.3[31]	531.4
O2	50.0	49.4	533.2[31]	533.1

of L-DOPA without significant contaminations on Au(110) surfaces after deposition runs as described above.

In detail, the following peak assignments have been made: the main peak at 284.5 eV contains contributions from two different components, the aromatic carbon (C1) at 284.5 eV and the aliphatic carbon (C2) at 285.1 eV. The C1 assignment agrees with a study by Solomon et al.[67] on phenol absorbed on Ag(110). They observed a peak at 284.4 ± 0.3 eV and assigned it to aromatic carbon. The binding energy difference of 0.6 eV between the aromatic and aliphatic carbon peaks is consistent with the difference observed for phenylene and alkyl species
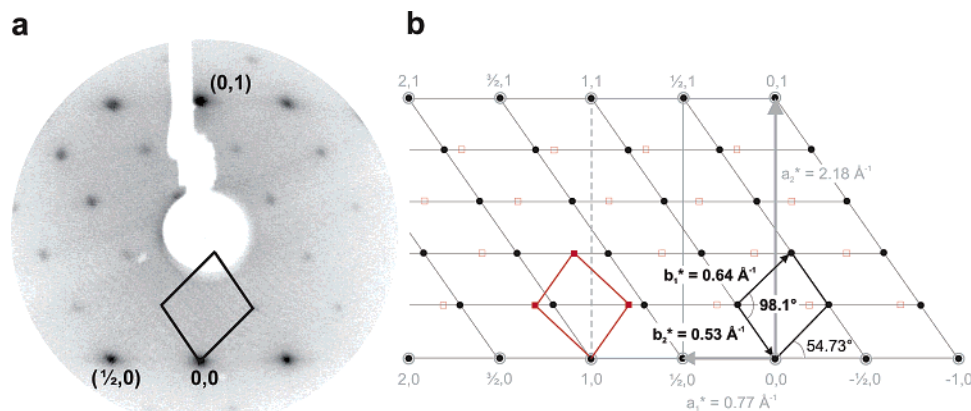
Figure 4. (a) LEED pattern of an L-DOPA film of 1.8 Å thickness on the (2 × 1) reconstructed Au(110) surface. The image was recorded at 40 eV electron beam energy. The surface was rotated out of normal incidence such that the 0,0 spot moves to the bottom of the screen. (b) Sketch of reciprocal space with diffraction spots of the reconstructed gold substrate (gray open circles, labeled with their diffraction order), the observed superstructure spots of the molecular adsorbate layer (black circles), and the superstructure spots (red open squares) which would be expected for the mirror domain of the observed superstructure. Reciprocal lattice vectors of the substrate lattice (gray) and the superstructure (black) and the unit cells of the observed (black) and its (not observed) mirror domain (red) are also shown. The gray dashed line indicates the unit cell of the unreconstructed Au(110) surface.

peaks in PDHPT (poly(2,5-diheptyl-1,4-phenylene-*alt*-2,5-thie-nylene)) on Si(110).[68] The second major experimental peak (at 286.1 eV) arises from two carbon species at almost identical binding energies: namely, the hydroxyl carbon (C3) at 286.1 eV and the carbon attached to the amino group (C4) at 286.2 eV. The assignment of C3 to the hydroxyl carbon is consistent with the studies of Petoral et al.[69] on tyrosin-terminated propanethiol on Au surfaces and Solomon et al.[67] on phenol, who observed hydroxyl C 1s at 286 and 285.9 eV, respectively. The assignment of C4 to the amino group is in agreement with the study by Petoral et al.[69] Finally, the C5 peak at 288.4 eV is assigned to carbon in the carboxylic group. On Pt(111), Löfgren et al.[31] observed the C 1s peak of the deprotonated carboxyl group in glycine at 289 eV. The agreement between our results for C5 and literature values is not as good as that for C1 to C4. This may indicate an interaction of the carboxyl group with the Au(110) surface. We note here that the charge state of CO_2^- will of course have a strong influence on the C 1s binding energy. Due to the interaction with the substrate, this charge state may change slightly, leading to small shifts of the C5 component. Finally, a shake-up line for the aromatic carbon ($\pi \rightarrow \pi^*$) was observed at about 291.8 eV, which is in agreement with the π-bond shake-up satellite for C 1s in polystyrene.[70]

We now turn to the O 1s results. The double peak structure suggests a fit with two components. However, attempts to fit the O 1s line with two components failed, as the agreement between the experimental line shape and the double-line fit is not satisfactory, and moreover the intensity ratio between the two fitted lines does not agree with the expected stoichiometry of oxygen species in L-DOPA. On the other hand, if two satellites are added to the two main lines, a good fit is obtained. The existence of strong satellites in O 1s spectra of oxygen atoms in conjugated environments has been observed in previous studies. It has been explained by excitations of valence electrons upon the sudden creation of a core hole.[71] The final peak fit of the O 1s core level is shown in Figure 3b.

In detail, the O 1s region features two main peaks at 531.4 and 533.1 eV. The O 1s peak at 531.4 eV is assigned to the oxygen of the carboxyl group; the satellite peak S1 at 532.3 eV is attributed to this carboxylic oxygen species. The second main component at 533.1 eV (O2) is assigned to the oxygen in the hydroxyl groups, and for reasons of stoichiometry the satellite S2 at 533.2 eV must be attributed to hydroxyl oxygen.

Our assignments of the main oxygen peaks agree with the results from oxidized carbon species in the literature,[31,69] where carbonyl/carboxyl oxygen was observed at 531.1/531.3 eV and hydroxyl oxygen at 533.2 eV.

A summary of all peak assignments is compiled in Table 1. In conclusion, the chemical composition of the film as measured in XPS confirms that these films consist of pure L-DOPA.

3.3. Structure of the Deposited Film. We now turn to a discussion of the structure of L-DOPA films on Au(110). Figure 4a shows a LEED pattern observed from a 1.8 Å layer of L-DOPA on Au(110). The layer thickness has been determined from XPS as described above. From both STM images and HREELS spectra to be discussed later, we know that the nominal layer thickness of 1.8 Å corresponds to a partial (i.e. submono-layer) coverage of the surface by compact monolayer islands. Submonolayer coverage is also confirmed by the coexistence of superstructure and substrate spots in LEED.

As expected, the surface topography of Au(110) acts as a template for the formation of ordered molecular layers. In fact, the LEED images prove the formation of a commensurate overlayer, by the periodic coincidence of substrate and super-structure spots. From the schematic plot of the diffraction pattern in Figure 4b the superstructure matrix (with respect to the reconstructed Au(110) surface) can be determined as

$$\begin{pmatrix} 1 & 2 \\ -1 & 3 \end{pmatrix} \tag{1}$$

This results in a real-space supercell with lattice constants b_1 = 9.99 Å, b_2 = 11.88 Å, and α = 98.1°, for a reconstructed Au(110) cell with a_1 = 8.16 Å and a_2 = 2.88 Å.

For higher coverages, we first observe an increased damping of substrate spots and then a complete attenuation of the superstructure spots (the latter are discernible for nominal layer thicknesses up to 7 Å). This can be explained by the completion of the L-DOPA monolayer and a subsequent loss of order in higher molecular layers, starting from the second layer. As will be argued below, the loss of order as early as in the second monolayer can be understood from the inconsistency of the monolayer and bulk crystal structures of L-DOPA. In line with the motivation of our work, we focus here on the structure of the monolayer, which allows us to gain insights into the molecule−surface interaction.

The Au(110) surface belongs to the 2D space group *pmm*, corresponding to full rectangular point symmetry. In particular, this group has two mutually perpendicular mirror planes normal to the surface. Since the superstructure shown in Figure 4 is lacking these mirror symmetries, we would expect the formation of mirror domains of L-DOPA on Au(110). For the superstructure matrix defined above in (1), four domains with two distinct LEED patterns would result (cf. Figure 4). Experimentally, however, only one domain is observed. This is naturally explained by the fact that L-DOPA is a chiral molecule, with its chiral center located at the carbon atom to which the amino group and the carboxyl group are attached (marked with a red solid arrow in Figure 1). Transition from the observed domain in Figure 4a to its mirror domain would involve a simultaneous transition from L-DOPA to D-DOPA. Because our films contain L-DOPA only, it is clear that only one domain can be observed. The monolayer of L-DOPA on Au(110) therefore establishes a chiral surface. One-domain interfaces have also been observed for other chiral molecular adsorbates.[53,72,73]

We note here that, in addition to its intrinsic chirality, L-DOPA acquires a second chiral center on adsorption. This chiral center is located at the carbon atom in the phenyl ring which connects the ring to the carbon chain (cf. the dashed arrow in Figure 1a). This surface-induced chiral center is a consequence of the asymmetric substitution of hydroxyl groups on the ring, asymmetric with respect to the C−C axis branching off the ring (red dashed line in Figure 1a). When the molecule adsorbs on the surface, the aromatic ring, being oriented parallel to the surface (see below), can bond in two inequivalent orientations, as Figure 1a,b shows, where the surface-adsorbed L,L-DOPA and L,D-DOPA molecules are depicted schematically. Here, the first letter refers to the intrinsic chirality of the molecule, while the second letter labels the surface-induced chirality. In principle, the additional chirality allows the formation of two distinct homochiral domains of L-DOPA on Au(110), if the two surface species L,L-DOPA and L,D-DOPA phase-separate on ordering. Alternatively, heterochiral islands with an equal number of L,D and L,L molecules may form. In our LEED experiments, we have observed no evidence for the segregation of the two phases. STM results to be discussed below, in fact, prove the formation of islands which are heterochiral with respect to the surface-induced chiral center.

We now turn to the vibrational properties of L-DOPA on Au-(110). Their detailed analysis allows us to gain important insights into the molecular structure and bonding of L-DOPA on Au-(110).

3.4. Vibrational Properties of L-DOPA Films on Au(110). From Figure 2, it is clear that the vibrational spectrum of L-DOPA is extremely rich. The molecule consists of 25 atoms, yielding $3N - 6 = 69$ normal-mode vibrations for the separate molecule. The bulk crystal contains two molecules per unit cell and thus has 144 normal modes. These modes come in pairs of two, for which the intramolecular displacement patterns are nearly identical; in one of these two modes the atomic displacements of the two molecules are in phase, and in the other they are out of phase. Because of the weak interaction between the two molecules, the predicted frequency split (Davydov split) between the two modes of any pair is in most cases very small (typically less than 10 cm^{-1}).

Because some of the normal modes are localized in distinct parts of the molecule, they can in principle be used for probing whether a certain molecular interaction potential is activated upon adsorption or not. For example, from the behavior of certain modes we may be able to conclude whether the

phenylene ring interacts with the Au surface or not. In the former case, we would expect to find the phenylene ring oriented parallel to the surface, while in the second case it may show a substantial tilt. Clearly, a detailed understanding of the experimentally observed modes for L-DOPA/Au(110) in terms of the corresponding displacement patterns is an essential prerequisite for analyzing the activity of the various molecular interaction potentials in this way. For this reason we now discuss the assignment of the experimentally observed vibration frequencies to the calculated eigenmodes of L-DOPA.

The first issue arising in this context is the question which of the two calculated spectra is most appropriate for L-DOPA/Au(110). We have argued in section 3.1 that the IR spectra of as-deposited L-DOPA multilayer films on KBr are better explained by calculations for the zwitterionic crystalline state. A priori, it is not clear whether the same is true for L-DOPA monolayers on Au(110). After all, the monolayer certainly does not consist of 3D crystallites, and even the zwitterionic nature of the molecule on the gold surface is not a default. However, it does turn out that the vibrational spectra of the zwitterionic modification also fit the HREELS data from the monolayer best. This certainly indicates a zwitterionic modification of L-DOPA on Au(110) (because any internal redistribution of the charge between the amino and acid groups will lead to large changes in the vibrational spectra), and it may even indicate that at least some of the structural motifs of the bulk phase are also present in the monolayer on Au(110). This last point will be discussed in detail once we consider which conclusions can be drawn from the vibrational modes as experimental probes of the molecule−molecule and the molecule−substrate interactions. Before this can be done, we must determine the correct mode assignments. In the following sections, theoretical mode frequencies are printed in *italics*, while experimental frequencies appear in the normal Roman type.

3.4.1. Mode Assignments. We will discuss the vibrational properties of the L-DOPA films on the basis of the deconvoluted HREELS spectra of Figure 5c,d (original HREELS spectra for submono- and multilayer coverage of L-DOPA on Au(110) are provided in the Supporting Information, where the as-measured and the deconvoluted spectra are displayed together; the residual is essentially structureless, indicating a successful deconvolution). The deconvolution has been conducted using the program package CUTTING EDGE.[74,75] The deconvolution with the experimentally determined instrument function yields a resolution enhancement of 2.3, resulting in a final resolution of the deconvoluted spectra of 1.8 meV. All features which can be considered as significant are labeled by their respective frequencies.

Figure 5b displays a calculated spectrum of the zwitterionic state. This spectrum has been broadened with Gaussians of 10 cm^{-1} width and then scaled with the scale factor 0.992, deduced from the R_P analysis (cf. section 2). (A figure presenting a detailed comparison of the calculated spectrum with an experimental one is available in the Supporting Information.)

Table 2 contains the assignments of the experimentally observed modes of the spectra c and d in Figure 2 and the spectra in Figure 5. While—due to possible inaccuracies of the calculated frequencies and intensities—it is not always possible to establish a one-to-one correspondence between the experimental and calculated peaks, it is nevertheless almost always possible to establish correspondence between peak groups in the experimental and theoretical spectra. These groups are indicated in Table 2 by horizontal lines. The highly resolved experimental spectrum of the L-DOPA dispersed in KBr shows
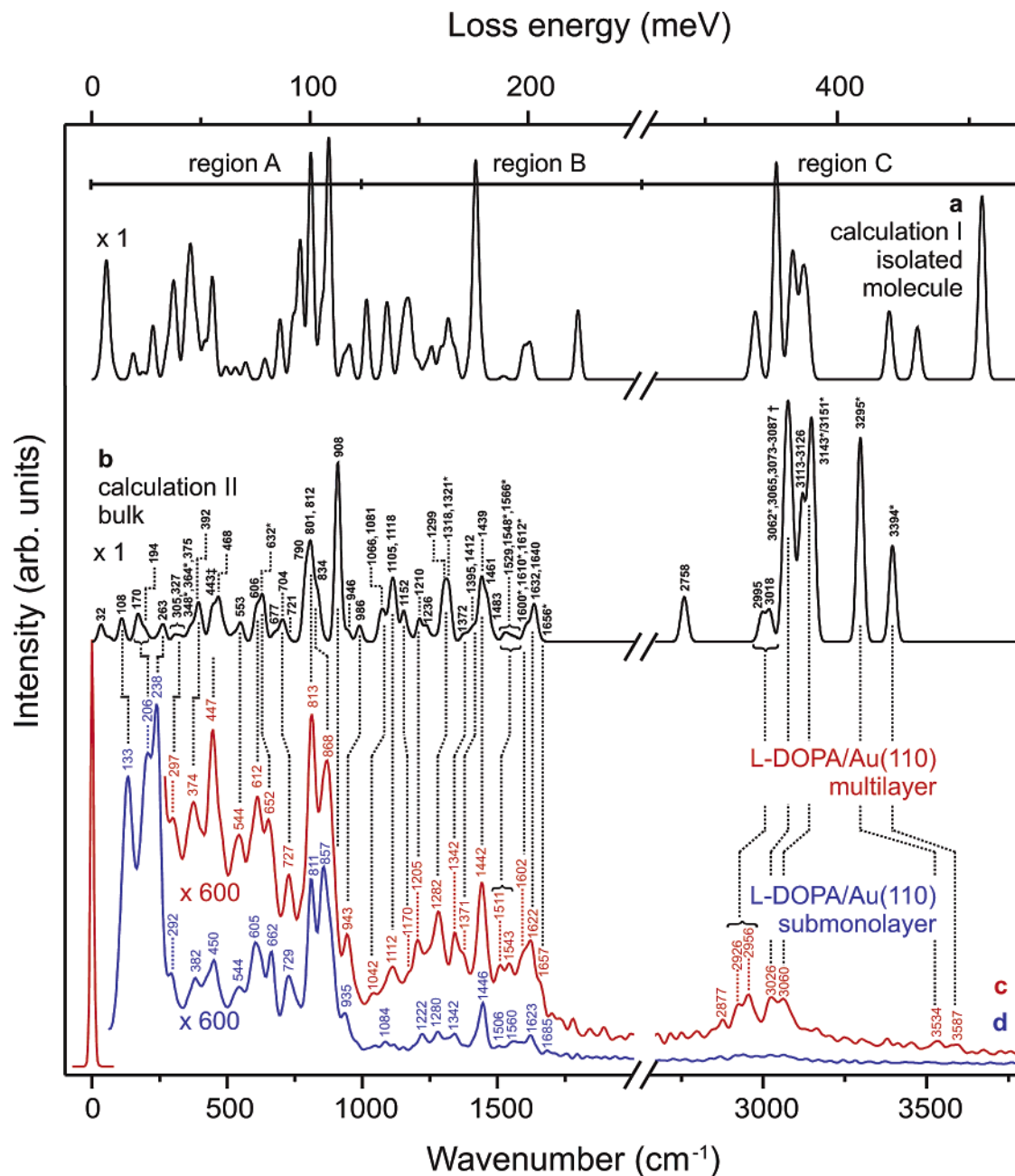
Figure 5. Detailed comparison of the experimental HREELS with DFT calculated vibrational spectra of L-DOPA. On the basis of this figure, the assignments in Table 2 have been made. (a) DFT calculation of the neutral state (same as in Figure 2a). (b) DFT calculation of the zwitterionic bulk state (same as in Figure 2b). (c) Experimental multilayer (6.7 Å) on Au(110) (deconvoluted HREELS spectrum, for original spectrum see Supplement Figure 1a). (d) Experimental submonolayer (1.8 Å) on Au(110) (deconvoluted HREELS spectrum, for original spectrum see Supplement Figure 1b). Vertical lines indicate the mode assignments of Table 2.

good resemblance with the theoretical spectrum and therefore also allows the identification of peaks in the other two not so well resolved spectra. We note that in most cases the calculated frequencies in Table 2 are the average between the frequencies of a Davydov-split pair. The corresponding intensity in the last column of Table 2 is the sum of the two mode intensities.

An analysis of the mode character in the various frequency regimes allows us to delineate three regions, which are clearly separated in the experimental spectra of Figure 5. In region A (from 0 to 1000 cm^{-1}) we mostly find low-frequency skeletal vibrations and modes with out-of-plane character, in particular out-of-plane ring deformation modes and wagging modes of the hydrogen atoms and hydroxyl groups on the ring and wagging modes of the carboxylate group. Just below 1000 cm^{-1}, the first in-plane deformation modes in the ring appear. In region

B (1000–1700 cm^{-1}), in-plane deformation and stretching modes of the ring are found; moreover, bending and stretching modes of its substituents as well as the chain and the carboxylate and amino groups are registered in this frequency range, with the exception of the hydrogen stretching modes, which are located in frequency region C (2700–3400 cm^{-1}).

In particular, we would like to draw attention to the following modes, because they play a role in the discussion of the molecular orientation at the interface L-DOPA/Au(110). At 813 and 868 cm^{-1} (multilayer) or 811 and 857 cm^{-1} (monolayer) the two strongest modes in the HREELS spectra are observed. They must be identified with out-of-plane wagging modes of hydrogen atoms of the ring or hydrogen atoms of the hydroxyl groups, predicted at *790*, *801*, *812*, *834*, and *908* cm^{-1} (here and in following the theoretical frequencies are shown in italics).

TABLE 2: Measured and Calculated (Zwitterionic State) Frequencies, Including Mode Assignments[a]

HREELS (multilayer)	IR (multilayer)	IR (bulk)	theory	assign	calcd intens[f]
			32	skeletal vib	9
			62[b]	skeletal vib	2
			108	skeletal vib	11
			170	skeletal vib	12
203			194	skeletal vib	5
238			223[b]	skeletal vib	1
297			247	skeletal vib	3
			263	skeletal vib	8
			305	skeletal vib	3
			327	skeletal vib	3
			348[b]	skeletal vib chain	2
374			364[b]	CO_2^- rocking + $\delta_s(CO_2^- -C-NH_3^+)$	5
			375	catechol ring torsion	3
			392	skeletal vib (catechol folding)	16
447			443[c]	skeletal vib (ring folding)	18
			468	skeletal vib (phenylene folding)	16
~ 480			490	NH_3^+ twist	6
	519		518	skeletal vib (ring torsion)	3
544	549	529→	539	skeletal vib	6
		554→	553	skeletal vib chain	5
		590→	606	oop ring deform	13
612	590	612→	632[b]	ip ring shear + $\omega(O-H)_{ring}$	20
		677→	669	$\omega(CO_2^-)$ + ring armchair mode	3
652		677→	669	$\omega(O-H)_{ring}$	3
		704→	696	ring armchair mode	10
727	721	719→	721	ip ring deform + $\omega(CO_2^-)$	3
		734			
		780→	790	$\omega(3\times C-H)_{ring}$ in phase + $\omega(C-CO_2^-)$	25
			801	$\omega(3\times C-H)_{ring}$ out of phase	18
	783	812→	812	$\omega(1\times C-H)_{ring}$	30
813	810	820			
868	819	839→	834	$\omega_s(H-O-C-H)_{ring}$	23
	874	868			
		922→	908	$\omega_{as}(H-C-C-H)_{ring}$	87
943	940	946→	946	ip ring deform + $\nu(C-C-C)_{chain}$ + $\delta(CO_2^-)$ scissor	5
	965	983→	986	$\nu(C-C-C)_{chain}$	8
		1065→	1066	$\nu(C-NH_3^+)$ + $\nu_s(CO_2^- -C-CH_2)$	11
			1081	$(C-H_2)_{chain}$ twist + ip ring deform	9
1112	~ 1060		1105	$\delta_s(H-C-H)_{ring}$	19
~ 1170	1117	1121→	1118	NH_3^+ rocking	22
	1154	1137→	1152	$\nu(catechol-chain)$	14
		1161→	1172	ip ring deform + $\nu_{as}(HO-C-C-OH)$	4
		1205→	1210	$\omega(H_2-C-CH-NH_3^+)_{chain}$	11
1205	1201	1232→	1236	$\nu_{as}(HO-C-C-OH)_{ring}$ + ip ring deform	8
	1263	1249			
		1256→	1260	$\nu_{as}(HO-C-C-OH)_{ring}$ + $(CH_2)_{chain}$ twist + ip ring deform	2
		1283→	1279[b]	$\delta_s(HO-C-C-OH)_{ring}$	2
1282	1287	1297→	1299	ring breathing	21
			1318	$\omega(H_2-C-CH-NH_3^+)_{chain}$ + ring breathing	10
			1321[b]	$\delta(NH_3^+-C-H)_{chain}$ scissor	12
1342	1330	1356→	1372	$\delta(C-H_2)_{chain}$ scissor	4
1371	1349	1384→	1395	$\nu_s(CO_2^-)$ + $\nu(C-CO_2^-)$	4
	1386	1407→	1412	$\nu_s(CO_2^-)$ + $\nu(C-CO_2^-)$	7
	1401	1441→	1439	$\nu(C=C)_{ring}$	30
1442	1445	1459→	1461	$\nu(C=C)_{ring}$	20
	~ 1500	1501→	1483	$\delta(NH_3^+)$ umbrella	4
1511		1528→	1529	$\nu(C=C)_{ring}$	5
1543	1516		1548[b]	$\nu_{as}(CO_2^-)$ + $\delta(NH_3^+)$	2
		1570→	1566[b]	$\delta(NH_3^+)$	2
		1592→	1600[b]	$\delta(NH_3^+)$	4
1602		1606→	1610[b]	$\delta(NH_3^+)$	3
1622	1600		1612[b]	$\nu_{as}(CO_2^-)$ + $\nu(C=C)_{ring}$	2
1657	1629	1632→	1632	$\nu(C=C)_{ring}$ + $\nu_{as}(CO_2^-)$	12
			1640	$\nu(C=C)_{ring}$	8
		1652→	1656[b]	$\nu_{as}(CO_2^-)$	1
	1739	1744			
2877	2853	2853	2758	$\nu(N-H)$	23
2926	2925	2924			
2956	2950-2960	~ 2958→	2995	$\nu(NH_3^+)$ 1H	14
		~ 2980→	3018	$\nu(C-H)_{chain}$	15
			3062[b]	$\nu(NH_3^+)$ 2H	29
		3070{	3065	$\nu(C-H)_{chain}$	15
3026	3000-3300		3073-3087[d]	$\nu(NH_3^+)$2H	36/38/43
3060			3113-3126[e]	$\nu(C-H)_{ring}$	13/12/21/19/5/4
		3200{	3143[b]/3151[b]	$\nu_{as+s}(O-H)_{meta}$	56/61
			3295[b]	$\nu_s(O-H)_{para}$	100
3534	3300-3500	3300-3500	3394[b]	$\nu_{as}(O-H)_{para}$	47
3587					

[a] The nomenclature follows that in ref 78. Abbreviations: ν, stretching vibration; δ, bending vibration; ω, wagging vibration; vib, vibration; ip, in-plane; oop, out of plane; s, symmetric; as, antisymmetric. Other mode characters are named explicitly. Due to the fact that the bulk unit cell contains two unit molecules, most modes are doubled. Unmarked entries in column 4 are the average frequency of two modes of equal character, one exhibiting an in-phase and the other an out-of-phase movement of atoms in both molecules. [c] Four modes. [b] One mode. [d] Three modes. [e] Six modes. [f] Arbitrary units.

We can thus conclude that both of the experimentally observed modes are associated with the catechol ring. The modes at *790*, *812*, and *834* cm^{-1} have in-phase character and should therefore have a strong dynamic dipole perpendicular to the catechol ring.

Another prominent mode is the one at 1442 (multilayer) or 1446 cm^{-1} (monolayer). This can be identified either with C=C stretching vibrations in the ring (calculated at *1439* and *1461* cm^{-1}) or with the umbrella mode of the amino group (*1483* cm^{-1}). As will be argued below, the second assignment seems more likely, although the calculated intensities of the C=C stretching modes in the ring are larger.

Other C=C stretching modes are predicted at *1299* cm^{-1} (the phenylene ring breathing mode) and *1632* cm^{-1}, the latter of which contains a component of antisymmetric carboxylate stretching character. Their experimental counterparts are found at 1282 and 1622 cm^{-1} in the multilayer.

Further characteristic modes in the HREELS spectrum are the modes at 1112 and 1205 cm^{-1}. The former may be assigned to the symmetric C−H bending vibration of the ring (predicted at *1105* cm^{-1}) or the NH$_3^+$ rocking vibration at *1118* cm^{-1}. The latter is either to be identified with a wagging mode of chain substituents (*1210* cm^{-1}) or the antisymmetric hydroxyl−phenylene stretching mode (*1236* cm^{-1}). Finally, the experimental spectrum exhibits a mode at 1342 cm^{-1}. This mode occurs in the vicinity of the calculated chain CH$_2$ scissor mode at *1372* cm^{-1}.

In the remainder of this section, we now employ some of the assigned modes as local probes and discuss the interaction of the various functional groups of the molecule with the substrate surface.

3.4.2. Orientation of L-DOPA on Au(110). In view of the overall aim of our work, i.e., understanding the bonding of L-DOPA to the Au(110) surface, the orientation of the phenylene ring with respect to the surface is of critical importance, because its π system is connected to some of the major molecular interaction potentials. Indeed, a ring orientation parallel to the surface would be strongly suggestive of a π interaction with the surface.

When the multilayer and monolayer spectra in Figure 5 are compared, the relative weakness of the modes in region B (often with displacements in the plane of the ring) of the monolayer spectrum is striking. In the frequency range of region A, the multilayer exhibits approximately twice the intensity of the monolayer spectrum, while in region B this ratio is closer to 4. This is true in particular for the modes at 1112, 1205, 1282, 1342, and 1622 cm^{-1}. The only exception to this general trend is presented by the mode at 1442 cm^{-1}. However, as mentioned above, this frequency may not be associated with the ring. Very likely, it belongs to the NH$_3^+$ umbrella vibration. The strong signal of this mode suggests that the NH$_3^+$ group of L-DOPA is tilted out of the surface plane, while the weak signals of the in-plane vibrations of the catechol ring (1112, 1205, 1282 cm^{-1}) and the C=C stretch (1622 cm^{-1}) indicate a flat orientation of the ring. Incidentally, the partial out-of-plane orientation of the NH$_3^+$ group is confirmed by the weak signal intensity of the NH$_3^+$ rocking mode, which may also contribute to the experimentally observed mode at 1112 cm^{-1}.

Further evidence of a flat phenylene ring in the monolayer is provided by the complete absence of the O−H stretching modes in region C at 3534−3587 cm^{-1}, whereas in the peak range of the C−H and N−H stretching vibrations some weak intensity remains.[80]

So far we have explained the relative suppression of modes at 1112, 1205, 1282, and 1622 cm^{-1} in the monolayer

in terms of a flat ring orientation. Similarly, it may be argued that the chain is nearly parallel to the surface, with the plane of the CH$_2$ group perpendicular to the surface. The suppression of the CH$_2$ scissor mode at *1372* cm^{-1} by its dynamic image dipole may hence account for the weakness of the experimental peak at 1342 cm^{-1} in the monolayer. The absence of the H$_2$−C-CH−NH$_3^+$ wagging mode, expected at *1210* and *1318* cm^{-1}, is consistent with such a chain orientation.

Having established the flat orientation of the catechol ring (and its concurrent surface interaction) as well as the tilted orientation of the NH$_3^+$ group (it is, however, as yet unclear whether this group points toward the surface or away from it), and having argued in favor of a perpendicular orientation of the plane of the CH$_2$ group to the surface, we can now proceed to an analysis of the two remaining functional groups, namely the carboxylate and the hydroxyl groups, and their surface interaction.

3.4.3. Vibrations of the Carboxylate Group. Discussing the acid group of L-DOPA adsorbed on Au(110), it must first be remembered that the absence of the C=O stretching mode at typically *1798* cm^{-1} provides clear evidence for the existence of a negatively charged, delocalized CO$_2^-$ group. On the basis of this observation, we will now discuss the orientation of the carboxylate group relative to the surface, as well as its interaction with the metal substrate.

If, as we have argued in the previous sections, the first two carbon−carbon bonds of the chain (starting at the ring) are parallel to the surface, either the amino group or the carboxylate group may point toward the surface. For steric reasons, it is impossible to have the hydrogen atom of the C atom marked with a solid red arrow in Figure 1 pointing either toward or away from the surface. Let us for the moment assume that the carboxylate group of L-DOPA interacts with the Au surface. This is indeed found for a number of other amino acids.[55]

The ionized carboxylate group supports two stretching vibrations, one of them symmetric, usually found in the frequency range 1380−1460 cm^{-1}, and the other antisymmetric, which is typically observed in the region 1580−1640 cm^{-1}. The polarization vectors of both modes are oriented perpendicular to each other. The relative intensities of these two modes, as well as possible frequency shifts, may be used to determine the way in which the carboxylate group interacts with a surface. Three configurations have been described in the literature: in the unidentate configuration, the plane of the carboxylate group is oriented perpendicular to the surface, and accordingly only one oxygen atom points toward the surface. For the so-called bidentate and bridging configurations, the acid plane may be either perpendicular or parallel to the surface. A nearly perpendicular orientation of the acid plane has been reported for other simple amino acids (glycine, alanine, serine) adsorbed on Cu(110)[33,76,77] and for cysteine adsorbed on Au(110).[53] In the case of the bidentate configuration, both oxygen atoms interact with the same metal atom, whereas in the case of the bridging configuration the carboxylate bridges two neighboring metal atoms.

In the zwitterionic bulk of L-DOPA, the asymmetric carboxylate stretching vibration is predicted at *1612/1656* cm^{-1}, whereas the symmetric stretch appears at *1412* cm^{-1} (in these modes the carboxylate stretching character is strongest). It must be noted that both modes have relatively small dynamic dipole moments (cf. Figure 5 and Table 2). In practice, they will therefore be obscured by strong neighboring modes. Fortunately, all these neighboring modes are polarized parallel to the plane of the phenylene ring (or−in the given configuration of the

molecule—to the surface), such that—at least in the monolayer—they should be almost totally suppressed. Despite their weakness, the CO_2^- stretching modes may therefore be detectable, if the orientation of the acid group itself allows this. For the unidentate configuration, one would expect the antisymmetric stretching mode to be favored. In contrast, for the two other configurations, the antisymmetric stretching vibration should be very weak, while the symmetric mode may or may not be strong, depending on the orientation of the acid plane in the bidentate or bridging configurations. Considering the monolayer spectrum in Figure 5, we can rule out the unidentate configuration with some certainty, because the spectrum shows no sign of the antisymmetric mode. Meanwhile, the symmetric mode may or may not contribute to the strong peak at 1446 cm^{-1} (monolayer). Because of the relatively close vicinity of the NH_3^+ umbrella mode and the CO_2^- symmetric stretching vibration, it is in fact impossible to determine the orientation of the acid plane in the bidentate or bridging geometries. However, considering the steric structure of the molecule, it seems most likely that the acid plane and the NH_3^+ group are tilted with respect to the surface plane. This may in fact indicate that the peak at 1446 cm^{-1} contains contribution from both the NH_3^+ umbrella mode and the symmetric carboxylate stretching vibration.

Finally, we note that a distinction between the bidentate and the bridging geometries may in favorable cases be concluded from the frequency difference between asymmetric and symmetric carboxylate stretching modes. The fact that neither of the two modes can be clearly identified in our monolayer spectra precludes this possibility in the present case.

3.4.4. Vibrations of the Hydroxyl Group. Finally, we turn to the hydroxyl groups. The most specific vibrational frequency of the hydroxyl group belongs to the internal O—H stretching vibration which is commonly observed between 3300 and 3600 cm^{-1}. Because hydroxyl groups have a propensity toward taking part in hydrogen bridge bonds, the frequency range in which O—H stretching vibrations are found is rather broad. If the hydrogen atom of an O—H group mediates the interaction with another electronegative atom, the internal O—H stretching vibration is shifted to lower frequencies than in those cases where no such interaction exists.[78,79] We can therefore use the O—H stretching vibration as a probe to learn about intermolecular hydrogen interactions.

As has been mentioned already in section 3.4.1, no O—H stretching vibrations are observed in the monolayer. This is to be expected if the phenylene ring lies flat on the surface and all O—H bonds in L-DOPA are strictly coplanar with the phenylene ring.

In previous work on L-DOPA adsorption on metal surfaces, namely Pt(100) and Pt(111)[16] and gold nanoparticles,[17] it was suggested that the molecule dehydrogenates at the hydroxyl groups on surface adsorption in the first monolayer. In the present case, such a dehydrogenation does not occur, as follows unambiguously from the observation of the out-of-plane internal O—H wagging mode at 857 cm^{-1} in the monolayer. This mode is in fact one of the strongest modes in the whole L-DOPA spectrum on Au(110). Note that we have assigned the experimental peak at 857 cm^{-1} to the ω_s(H—O-C-C—H)$_{ring}$ mode at *834* cm^{-1} rather than to the antisymmetric H—C-C—H wagging mode at *908* cm^{-1}, because the latter should not show a strong intensity if the catechol ring is oriented parallel to the surface.

In multilayers of L-DOPA on Au(110), O—H stretching modes are experimentally observed at approximately 3500 cm^{-1}, whereas the calculation places them at lower frequencies (around *3350* cm^{-1}) in the zwitterionic bulk and at higher frequencies

(around *3600* cm^{-1}) for the separate neutral molecule. This is in sharp contrast to the C—H stretching modes, which are found to be in rather good agreement with the zwitterionic calculation. It is clear why the zwitterionic crystal has a low O—H stretching frequency: according to Figure 1, each of the hydroxyl groups in the L-DOPA crystal participates in a hydrogen bridge bond. Since we know that the molecule on Au(110) is still zwitterionic (in the monolayer as well as in the multilayer), the blue shift of the internal hydroxyl stretching frequency suggests that the multilayer molecules on Au(110), and in particular their hydroxyl groups, are involved in fewer hydrogen bonds than in the zwitterionic crystal, even in multilayers.

3.5. Real-Space Imaging of L-DOPA on Au(110). We now turn to the analysis of STM images of L-DOPA monolayers on Au(110). As mentioned before, the STM experiments were carried out in a different vacuum chamber than for all experiments discussed up to this point. After deposition at room temperature, the sample was cooled to 10 K. During cooling to 100 K, LEED images were recorded, and no changes in the LEED image have been observed. In the STM, we found the expected submonolayer coverage of L-DOPA on Au(110). The surface revealed compact, ordered monolayer islands next to uncovered substrate areas, exhibiting the (2 × 1) reconstruction of Au(110).

Two STM images are displayed in Figure 6. Although we have scanned large areas of the surface, only the structure shown in the two images of Figure 6 has been found. In panel a, the Au surface as well as a monolayer island of L-DOPA is visible. The distance between the vertical lines in the upper left part of the image fits very well to the distance between the (2 × 1) reconstructed metal rows. On these rows, we observe bright, nearly circular features of approximately 5 Å diameter. Comparing this diameter to the size of the molecule, we can conclude that these features correspond to one molecule each. We note that no change of the metal reconstruction close to the islands of L-DOPA is discernible. Because close to the island boundary the molecular islands show some irregularities in the lateral positions of the molecules, we now turn to an image which was taken inside a large molecular island (Figure 6b). This image exhibits strict two-dimensional periodicity. If the unit cell deduced from this image (b_1 = 9.8 Å, b_2 = 11.5 Å, θ = 100°) is compared to the cell based on LEED experiments, we find a very good agreement. Analyzing the molecular arrangement in more detail, we find two kinds of dimerizations in the layer. First, we observe a clear pairing of the two molecules labeled A in Figure 6b. Second, a weaker pairing is also observed along the [1$\bar{1}$0] directions of the Au(110) atoms rows (labeled B). As will be argued below, these dimerizations provide important clues concerning the exact arrangement of the molecules in the superstructure unit cell. This will be discussed in the next section, in light of all available data from diffraction, spectroscopy, and microscopy experiments.

3.6. Structural Model for L-DOPA on Au(110). In this section a structural model for the L-DOPA/Au(1110) interface is proposed. From the various experimental methods, the following experimental facts have been extracted in the previous sections.

(1) Pure L-DOPA exists on Au(110) in its zwitterionic state.

(2) L-DOPA forms a commensurate superstructure on the (2 × 1)-reconstructed Au(110) surface, most probably leaving the substrate reconstruction intact.

(3) The phenylene ring (and consequently the hydroxyl groups) are oriented parallel to the surface.
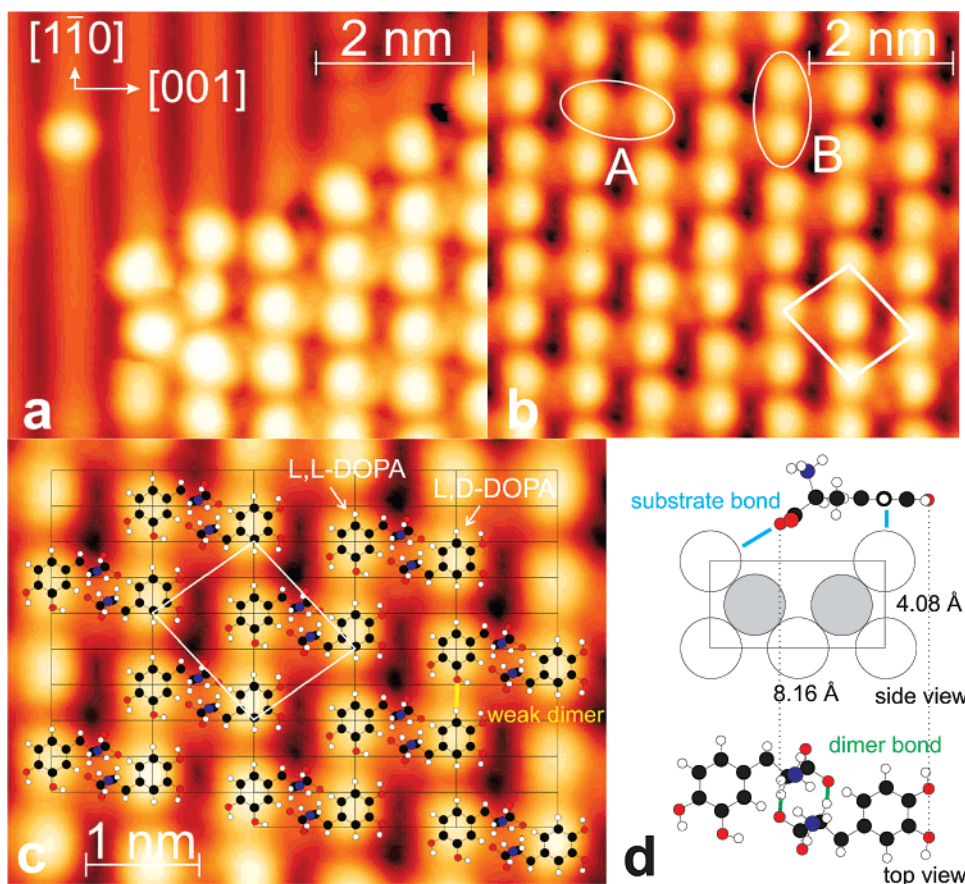
(4) Although the superstructure breaks the *pmm* symmetry

Figure 6. STM images recorded from a submonolayer L-DOPA/(2 × 1)Au(110) film structure model. All images were scanned with 313 mV bias voltage and 7.5×10^{-11} A tunneling current. (a) Image (size 6.1×5.3 nm^2) taken close to the boundary of a L-DOPA island. In the upper left-hand part of the image the ridges and grooves of the reconstructed Au surface are visible. (b) Image (size 6.5×5.7 nm^2) recorded inside a large L-DOPA island. The superstructure unit cell ($b_1 = 9.8$ Å, $b_2 = 11.5$ Å, $\theta = 100°$) is shown in white. Two types of dimerizations (A, B) are indicated (see the text). (c) Enlarged section of image b, with (2 × 1) reconstructed unit cell (black lines) and superstructure unit cell (white lines). The aspect ratio of the STM image has been corrected to yield the correct geometry of the superstructure unit cell (1.37% expansion in the *y* direction). The structure model projected into the image is discussed in the main text. (d) Side view of L-DOPA on the (2 × 1) reconstructed Au(110) surface (top) and top view of a dimer from part c. In parts c and d various intermolecular and molecule substrate bonds are indicated in yellow, blue, and green; see the text for a detailed discussion.

of the substrate, only one domain is observed in STM and LEED, despite the presence of two distinct surface species L,D- and L,L-DOPA.

(5) The O···O axis of the carboxylate group is oriented parallel to the surface (bidentate or bridging configuration).

(6) Both the central axis of the NH$_3^+$ group and the plane of the carboxylate group are tilted out of the surface plane. In principle, it is not clear whether the amino group or the carboxylate group faces the gold surface.

(7) In the ordered structure, the hydroxyl groups of L-DOPA are not dehydrogenated.

(8) In the multilayer on Au(110), L-DOPA molecules have fewer hydrogen bridge bonds than in the zwitterionic bulk crystal. The interface to Au(110) therefore does not support the growth of crystalline thin films in the bulk structure of L-DOPA.

(9) The molecules arrange in rows on top of the ridges of the (2 × 1) reconstructed Au(110) surface.

(10) Along the [001] direction, i.e., perpendicular to the gold ridges, the molecules form dimers.

(11) Along the [1$\bar{1}$0] direction, i.e., parallel to the gold ridges, a weaker dimerization is observed.

On the basis of these observations, we have developed a structural model for the arrangement of the molecules in the unit cell. This model is projected into the experimental image in Figure 6c. In combination with the steric structure of the

molecule, which includes its ability to form various configurations by rotation around single σ bonds, the listed experimental facts establish stringent constraints for the actual structure of the L-DOPA monolayers on Au(110) which we have studied in the present work, without the need for many additional postulates. In fact, in constructing Figure 6c,d we have made the following additional well-motivated assumptions.

(1) We have assumed that the phenylene ring is centered, or nearly centered, on the atomic ridges of the (2 × 1) reconstructed Au(110) surface. In other words, we have assumed that the feature appearing brightest in the STM image of a L-DOPA molecule is the catechol ring with its large density of states in the π-electron system. This assignment is also made plausible by the measured size of the bright feature.

(2) We have assumed a head-to-head and tail-to-tail arrangement of the molecules along the main dimerization direction. Both the bulk structure of L-DOPA and the observed dimerization itself speak in favor of this conjecture. Furthermore, we have assumed that the carboxylate group points toward the metal surface.

(3) The fact that only one domain is visible, despite the existence of both L,D- and L,L-DOPA on the surface, is naturally explained by assuming that this domain is a 1:1 mixed phase of L,D- and L,L-DOPA. While it is very difficult, if not impossible, to distinguish the two species in the STM image,

the postulated existence of a mixed phase very naturally explains the second, weaker dimerization which is clearly observed (see below).

The molecular arrangement can thus be described as follows: the phenylene ring adsorbs atop the ridge, while the chains from molecules on neighboring ridges point toward each other and interlock with hydrogen bonds. As demonstrated by the schematic plot in Figure 6c, the chains fit well to each other if the two carboxylate groups point toward the surface. We thus interpret the increased local density of states between two phenylene rings on neighboring atomic ridges as originating from the electronic states in the carbon chains and amino groups of the two molecules forming a dimer. In this model, the strong dimerization is effected by the attractive intermolecular interactions between the chains of two molecules (Figure 6d). However, the interlocking of the chains is not the only intermolecular interaction observed in this model. A second interaction exists between the oxygen atom of one of the two hydroxyl groups and the hydrogen atom on the ring of a neighboring molecule. If, as has been done in Figure 6c, the main dimers are formed by one molecule each of type L,D- and L,L-DOPA, such bridges must exist in exactly those places which show a slightly higher intensity of local density of states between neighboring molecules along the ridge direction. This faint intensity is therefore ascribed to the presence of a hydroxyl group in the space between two phenylene rings. Remarkably, the side view of the structure (Figure 6d) reveals a good structural match between the groove structure of the (2 × 1) reconstructed Au(110) surface and the three-dimensional structure of the L-DOPA molecule.

We finally note that although all observed facts are naturally explained by this model, we cannot say for certain that the proposed model is indeed correct. While the proposed model is a synthesis of all experimentally available facts, it does not replace a quantitative surface structure analysis by diffraction methods or density functional theory.

4. Conclusions

In this paper we have analyzed the structural and vibronic properties of L-DOPA monolayers on a model surface, namely Au(110), with the aim of evaluating the activity of various molecular interaction potentials (MIP) upon adsorption of the amino acid on a metal surface. As expected, we have found that the structure of the reconstructed surface leads to a strong templating effect. The ensuing order in the molecular layer has allowed us to access important parameters of the intermolecular and molecule−substrate interactions. A structural model based on these parameters has been developed and discussed.

On the basis of this structural model, we can conclude that L-DOPA interacts with the gold substrate via two of its functional units, the phenylene ring and the carboxylate group. The interaction potentials involved in the interaction of the ring with the metal surface may be charge transfers (chemical interaction), the polarizability of the π-electron system (physisorption), or a combination of both. At the carboxylate group, on the other hand, the negative charge, the associated dipole moment, and the reactivity of oxygen toward metals may play a role in the metal−molecule interaction. Other groups of the L-DOPA molecule are predominantly involved in the intermolecular interactions between L-DOPA molecules. This is true for the H-acceptor and H-donor potentials at the charged amino and carboxylate groups and the neutral hydroxyl groups.

If the interaction of L-DOPA-containing peptides and proteins with metal surfaces is considered, it must be noted that the interaction of the carboxylate group with the surface is not an option, because this group (as well as the NH_3^+ group) takes part in the biopolymerization reaction forming the peptide or protein backbone. The interaction with the substrate will therefore rely on the interaction potentials of the phenylene ring. Its role for the adhesion can hence be envisaged as that of a surface anchor. Via its hydroxyl groups, this ring may also support intermolecular interactions between neighboring surface anchors, as has been observed in the present case of an ordered L-DOPA layer on our model Au(110) surface. Finally, we note that the role of the catechol ring as a surface anchor in the protein surface interaction establishes a *second* important function of the catechol ring of L-DOPA in the surface adhesion of DOPA-containing proteins: it was already mentioned that the hydroxyl groups of the catechol ring, after dehydrogenation, allow the complexation with metal ions.[18,19] It thus appears that the catechol ring plays a twofold role in the adhesive mussel protein: its aromatic ring functions as a surface anchor and thus enables the surface adhesion of the protein, while the substituted hydroxyl groups support the curing of the adhesive protein in wet environments. One can thus conclude that the double functionality of the catechol ring in L-DOPA is a key contribution to the adhesive properties of mussel glue.

Supporting Information Available: The results of our SIESTA ab initio calculations for bulk L-DOPA, provided as a supplement consisting the file "L-DOPA Bulk Calculations.pdf" and a set of XYZ files. In the PDF file the frequencies of all vibrational modes of bulk L-DOPA are listed together with the corresponding normalized intensities. The XYZ-files contain the displacement patterns of the normal modes. Molecular oscillations can be visualized with the program GOPENMOL, which is freely available. Loading of XYZ files and visualization of normal mode vibrations proceed as follows. (1) Download a free version of GOPENMOL from http://www.csc.fi/gopenmol/. (2) Start the program by running the batch file. (3) Import atomic coordinates, using File → Import → Coords..., → Browse. Choose any XYZ file from the correspondending folder and press Apply. A new window with skeletons of two L-DOPA molecules (unit cell of bulk L-DOPA) will appear. (4) Import the vibration trajectory, using Trajectory → Main..., → Browse. Choose the XYZ file of the required vibrational mode (cf. the PDF file for its frequency, e.g. "100.xyz") Press the Import and | > button. Molecules will start to oscillate. (5) For better visualization, the oscillation speed may be adjusted in the Slow display field: e.g., with a value of 100. (6) If desired, rotate the unit cell with the mouse cursor. Additionally two figures are provided as supplement in the PDF-file Supplement Figures.pdf. The first one presents original HREELS spectra from multi- and submonolayer films of L-DOPA on Au(110) and their deconvolutions. The second contains a detailed comparison between the broadened calculated spectrum for the zwitterionic bulk state of L-DOPA and the FT-IR spectrum of sublimated L-DOPA. This material is available free of charge via the Internet at http://pubs.acs.org.

References and Notes

(1) Waite, J. H. *Biol. Rev. Cambridge Philos. Soc.* **1983**, *58*, 209.
(2) Waite, J. H. *Int. J. Adhes. Adhes.* **1987**, 7, 9.
(3) Yule, A.; Walker, G. *J. Mol. Biol. Assoc. U.K.* **1984**, *64*, 147.
(4) Cook, M. *Adhesion in Biological Systems*; Manley Academic Press: New York, 1970.
(5) Brown, C. *Q. J. Microsc. Sci.* **1952**, *93*, 487.
(6) Waite, J. H.; Tanzer, M. *Science* **1981**, *212*, 1038.

(7) Waite, J. H. *J. Biol. Chem.* **1983**, *258*, 2911.

(8) Waite, J. H.; Housley, T.; Tanzer, M. *Biochemistry* **1985**, *24*, 5010.

(9) Inoue, K.; Takeuchi, Y.; Miki, D.; Odo, S. *J. Biol. Chem.* **1995**, *270*, 6698.

(10) Papov, V.; Diamond, T.; Biemann, K.; Waite, J. H. *J. Biol. Chem.* **1995**, *270*, 20183.

(11) Waite, J. H.; Qin, X.-X. *Biochemistry* **2001**, *40*, 2887.

(12) Yu, M.;, Deming, T. *Macromolecules* **1998**, *31*, 4739.

(13) Waite, J. H. *Comp. Biochem. Physiol.* **1998**, *97B*, 19.

(14) Waite, J. H. *Biol. Bull.* **1992**, *183*, 178.

(15) Olivieri, M.; Baier, R.; Loomis, R. *Biomaterials* **1992**, *14*, 1000.

(16) Stern, D.; Hubbard, A. *Langmuir* **1988**, *4*, 711.

(17) Ooka, A.; Garrell, R. *Biopolymers* **2000**, *57*, 92.

(18) Monahan, J.; Wilker, J. J. *Chem. Commun.* **2003**, 1672.

(19) Taylor, S. W.; Chase, D. B.; Emptage, M. H.; Nelson, M. J.; Waite, J. H. *Inorg. Chem.* **1996**, *35*, 7572.

(20) Jastorff, B.; Stoermann, R.; Woelcke, U. *Struktur-Wirkungs-Denken in der Chemie*; Universitätsverlag Aschenbeck und Isensee: Bremen, Oldenburg, Germany, 2003.

(21) Jastorff, B.; Störmann, R.; Ranke, J.; Mölter, K.; Stock, F.; Oberheitmann, B.; Hoffmann, W.; Hoffmann, J.; Nüchter, M.; Ondruschka, B.; Filser, J. *Green Chem.* **2003**, *5*, 136.

(22) Noonan, J. R.; Davis, H. L. *J. Vac. Sci. Technol.* **1979**, *16*, 587.

(23) Lozovoi, A. Y.; Alavi, A. *Phys. Rev. B* **2003**, *68*, 245416.

(24) Tsubai, M.; Takenishi, T.; Nakamara, A. *Spectrochim. Acta* **1963**, *19*, 271.

(25) Itaka, Y. *Acta Crystallogr.* **1960**, *13*, 35.

(26) Howard, S.; Hursthouse, M.; Lehmann, C. *Acta Crystallogr., Sect. B* **1995**, *51*, 328.

(27) Humblot, V.; Méthivier, C.; Pradier, C.-M. *Langmuir* **2006**, *22*, 3089.

(28) Junk, G.; Svec, H. *J. Am. Chem. Soc.* **1963**, *85*, 839.

(29) Debies, T.; Rabalais, J. *J. Electron Specrosc. Relat. Phenom.* **1974**, *3*, 315.

(30) Pearson, F.; Slifkin, M. *Spectrochim. Acta, Part A* **1972**, *28*, 2403.

(31) Löfgren, P.; Krozer, A.; Lausmaa, J.; Kasemo, B. *Surf. Sci.* **1997**, *370*, 277.

(32) Löfgren, P.; Chakarov, D. V.; Kasemo, B. *J. Vac. Sci. Technol. A* **1998**, *16*, 2961.

(33) Barlow, S. M.; Kitching, K. J.; Haq, S.; Richardson, N. V. *Surf. Sci.* **1998**, *401*, 322.

(34) Hasselstrom, J.; Karis, O.; Weinelt, M.; Wassdahl, N.; Nilsson, A.; Nyberg, M.; Pettersson, L. G. M.; Samant, M. G.; Stohr, J. *Surf. Sci.* **1998**, *407*, 221.

(35) Booth, N. A.; Woodruff, D. P.; Schaff, O.; Giessel, T.; Lindsay, R.; Baumgartel, P.; Bradshaw, A. M. *Surf. Sci.* **1998**, *397*, 258.

(36) Chen, Q.; Frankel, D. J.; Richardson, N. V. *Surf. Sci.* **2002**, *497*, 37.

(37) Nyberg, M.; Hasselström, J.; Karis, O.; Wassdahl, N.; Weinelt, M.; Nilsson, A.; Pettersson, L. G. M. *J. Chem. Phys.* **2000**, *112*, 5420.

(38) Efstathiou, V.; Woodruff, D. P. *Surf. Sci.* **2003**, *531*, 304.

(39) Nyberg, M.; Odelius, M.; Nilsson, A.; Pettersson, L. G. M. *J. Chem. Phys.* **2003**, *119*, 12577.

(40) Tzvetkov, G.; Koller, G.; Zubavichus, Y.; Fuchs, O.; Casu, M. B.;, Heske, C.; Umbach, E.; Grunze, M.; Ramsey, M. G.; Netzer, F. P. *Langmuir* **2004**, *20*, 10551.

(41) Zubavichus, Y.; Shaporenko, A.; Grunze, M.; Zharnikov, M. *J. Phys. Chem. A.* **2005**, *109*, 6998.

(42) Williams, J.; Haq, S.; Raval, R. *Surf. Sci.* **1996**, *368*, 303.

(43) Zhao, X. Y.; Zhao, G. R.; Yang, W. S. *Surf. Sci.* **1999**, *442*, L995.

(44) Barlow, S. M.; Louafi, S.; Le Roux, D.; Williams, J.; Muryn, C.; Haq, S.; Raval. R. *Surf. Sci.* **2005**, *590*, 243.

(45) Jones, G.; Jones, L. B.; Hibault-Starzyk, F.; Seddon, E. A.; Raval, R.; Jenkins, S. J.; Held, G. *Surf. Sci.* **2006**, *600*, 1924.

(46) Barlow, S. M.; Louafi, S.; Le Roux, D.; William, J.; Muryn, C.; Haq, S.; Raval, R. *Langmuir* **2004**, *20*, 7171.

(47) Egawa, C.; Iwai, H.; Kabutoya, M.; Oki, S. *Surf. Sci.* **2003**, *532*, 233.

(48) Sayago, D. I.; Polcik, M.; Nisbet, G.; Lamont, C. L. A.; Woodruff, D. P. *Surf. Sci.* **2005**, *590*, 76.

(49) Iwai, H.; Tobisawa, M.; Emori, A.; Egawa, C. *Surf. Sci.* **2005**, *574*, 214.

(50) Rankin, R. B.; Sholl, D. S. *Surf. Sci.* **2005**, *574*, L1.

(51) Mateo Marti, E.; Barlow, S. M.; Haq, S.; Raval, R. *Surf. Sci.* **2002**, *501*, 191.

(52) Fleming, G. J.; Idriss, H. *Langmuir* **2005**, *20*, 7540.

(53) Kühnle, A.; Linderoth, T.; Hammer, B.; Besenbacher, F. *Nature (London)* **2002**, *415*, 891.

(54) Kühnle, A.; Molina, L. M.; Linderoth, T. R.; Hammer, B.; Besenbacher, F. *Phys. Rev. Lett.* **2004**, *93*, 0861011.

(55) Barlow, S.; Raval, R. *Surf. Sci. Rep.* **2003**, *50*, 201.

(56) www.casaxps.com.

(57) Mohai, M. *Surf. Interface Anal.* **2004**, *36*, 828.

(58) Wagner, C. D.; Davis, L. E.; Zeller, M. V.; Taylor, J. A.; Raymond, R. H.; Gale, L. H. *Surf. Interface Anal.* **1981**, *3*, 211.

(59) Shirley, D. *Phys. Rev.* **1972**, *55*, 4709.

(60) Ibach, H.; Mills, D. L. *Electron Energy Loss Spectroscopy and Surface Vibrations*; Academic Press: New York, 1982.

(61) Dunning, T. H. *J. Chem. Phys.* **1989**, *90*, 1007.

(62) Frisch, M. J.; Trucks, G. W.; Schlegel, H. B.; Scuseria, G. E.; Robb, M. A.; Cheeseman, J. R.; Montgomery, J. A., Jr.; Vreven, T.; Kudin, K. N.; Burant, J. C.; Millam, J. M.; Iyengar, S. S.; Tomasi, J.; Barone, V.; Mennucci, B.; Cossi, M.; Scalmani, G.; Rega, N.; Petersson, G. A.; Nakatsuji, H.; Hada, M.; Ehara, M.; Toyota, K.; Fukuda, R.; Hasegawa, J.; Ishida, M.; Nakajima, T.; Honda, Y.; Kitao, O.; Nakai, H.; Klene, M.; Li, X.; Knox, J. E.; Hratchian, H. P.; Cross, J. B.; Bakken, V.; Adamo, C.; Jaramillo, J.; Gomperts, R.; Stratmann, R. E.; Yazyev, O.; Austin, A. J.; Cammi, R.; Pomelli, C.; Ochterski, J. W.; Ayala, P. Y.; Morokuma, K.; Voth, G. A.; Salvador, P.; Dannenberg, J. J.; Zakrzewski, V. G.; Dapprich, S.; Daniels, A. D.; Strain, M. C.; Farkas, O.; Malick, D. K.; Rabuck, A. D.; Raghavachari, K.; Foresman, J. B.; Ortiz, J. V.; Cui, Q.; Baboul, A. G.; Clifford, S.; Cioslowski, J.; Stefanov, B. B.; Liu, G.; Liashenko, A.; Piskorz, P.; Komaromi, I.; Martin, R. L.; Fox, D. J.; Keith, T.; Al-Laham, M. A.; Peng, C. Y.; Nanayakkara, A.; Challacombe, M.; Gill, P. M. W.; Johnson, B.; Chen, W.; Wong, M. W.; Gonzalez, C.; Pople, J. A. *Gaussian 03*, revision C.02; Gaussian, Inc.: Wallingford, CT, 2004.

(63) Ordejón, P.; Artacho, E.; Soler, J. M. *Phys. Rev. B* **96**, *53*, R10441.

(64) Soler, J. M.; Artacho, E.; Gale, J. D.; García, A.; Junquera, J.; Ordejón, P.; Sánchez-Portal, D. *J. Phys.: Condens. Matter* **2002**, *14*, 2745.

(65) Pendry, J. B. *J. Phys. C: Solid State Phys.* **1980**, *13*, 937.

(66) Van Hove, M. A.; Weinberg, W. H.; Chan, M. C. *Low-Energy Electron Diffraction*; Springer-Verlag: Berlin, 1986.

(67) Solomon, J.; Madix, R.; Stöhr, J. *Surf. Sci.* **1991**, *255*, 12.

(68) Fahlmann, M.; Birgersson, J.; Kaeriyama, K.; Salaneck, W. R. *Synth. Met.* **1995**, *75*, 223.

(69) Petoral, R.; Uvdal, K. *J. Electron Spectrosc. Relat. Phenom.* **2003**, *128*, 159.

(70) *Handbook of X-ray Photoelectron Spectroscopy*; Moulder, J., Stickle, W., Sobol, P., Bomben, K., Chastain, J., Eds.; Physical Electronics Division, Perkin-Elmer: Eden Prairie, MN, 1995.

(71) Schöll, A.; Zou, M. J. Y.; Schmidt, T.; Fink, R.; Umbach, E. *J. Chem. Phys.* **2004**, *121*, 10260.

(72) Atanasoska, L.; Buchholz, J.; Somorjai, G. *Surf. Sci.* **1978**, *72*, 189.

(73) Lorenzo, M.; Baddeley, C.; Muryn, C.; Raval, R. *Nature (London)* **2000**, *404*, 376.

(74) Frederick, B. G.; Nyberg, G. L.; Richardson, N. V. *J. Electron Spectrosc. Relat. Phenom.* **1993**, *825*, 64.

(75) Frederick, B. G.; Frederick, B. B.; Richardson, N. V. *Surf. Sci.* **1996**, *368*, 82.

(76) Bowker, M.; Madix, R. *Appl. Surf. Sci.* **1981**, *8*, 299.

(77) Bao, S.; Liu, G.; Woodruff, D. *Surf. Sci.* **1988**, *89*, 203.

(78) Hesse, M.; Meier, H.; Zeeh, B. *Spektroskopische Methoden in der organischen Chemie*; Georg Thieme Verlag: Stuttgart, Germany, 1991.

(79) Davis, D.; Barteau, M. *Langmuir* **1989**, *5*, 1299.

(80) Note, however, that if the O−H bond is rotated out of the plane of the catechol ring, this argument is not valid. Clearly, the absence of the O−H stretching peak in the vibronic spectrum indicates a horizontal orientation of this particular bond only.